

Experimental Correlation of Installation Effects on Inlet Pressure Recovery

W. H. BALL* AND P. A. ROSS†
The Boeing Company, Seattle, Wash.

An extensive wind-tunnel investigation was conducted to determine airplane installation effects on isolated inlet performance. This investigation was accomplished by a series of tests involving several models to determine a) isolated inlet component internal performance, b) forebody flowfield, and c) installed inlet/forebody internal performance. The airplane system application for the results was a multimission strategic airplane. A semiempirical approach is developed which relates the isolated component performance of the inlet to the flowfield properties in the vicinity of its location on the airplane. Influence coefficients involving rates of change of inlet recovery with uniform changes in local flow properties such as Mach number, upwash, and sidewash and for induced gradients in Mach number are derived from the isolated inlet tests. These are then combined with the average local flow properties measured on the forebody to predict the installed inlet recovery. The comparison of predicted and measured installed inlet recovery suggests that experimentally derived influence coefficients obtained from component research can be used for airplane design accountability.

Nomenclature

A_c = inlet capture area
 A_∞ = freestream tube area
 M_∞ = freestream Mach number
 P_T = total pressure
 W = airflow rate
 α = angle of attack
 δ = pressure ratio to standard pressure
 ε = sidewash angle
 θ = temperature ratio to standard temperature
 σ = upwash angle
 ψ = yaw angle

Subscripts

2 = compressor face station
 ∞ = freestream

Introduction

PAST aircraft development programs have shown that it is necessary to adequately account for installation effects in arriving at realistic inlet performance predictions. This is especially true for highly integrated and multimission aircraft. The usual procedure occurring during the development process is to test the inlet installed on the fuselage (and wing, if required), compare the measured performance with design goals, and then iterate on the arrangement and component designs until satisfactory installed performance levels are obtained. This process is time-consuming and expensive; and it is often difficult to predict when and if success will be achieved. It also does not provide an understanding of the phenomena that cause the installation losses, because time and funding usually are not available to thoroughly analyze the experimental data and account for the observed occurrences. The problem is further complicated because the instrumentation used to measure installed inlet performance usually is not adequate to provide the data needed to develop a fundamental understanding of the problem.

Presented as Paper 71-759 at the AIAA/SAE 7th Propulsion Joint Specialist Conference, Salt Lake City, Utah, June 14-18, 1971; submitted June 28, 1971; revision received April 19, 1972.

Index category: Subsonic and Supersonic Airbreathing Propulsion.

* Senior Specialist/Engineer, Aeropropulsion Engineering, Aerospace Group.

† Senior Group Leader, Aeropropulsion Engineering, Aerospace Group. Member AIAA.

Recognizing these facts, a joint aeropropulsion wind-tunnel approach was adopted in Boeing strategic airplane studies to quickly provide essential data for integration of inlet and airplane. This paper describes the techniques used and the results obtained from an extensive series of wind-tunnel tests of $\frac{1}{20}$ scale models. These tests were designed to yield—in a related fashion—flowfield definition, inlet internal performance and inlet/airplane drag as a function of inlet position, forebody shape, and orientation. Drag data were measured during the tests, but they are not included in the scope of this paper; only inlet internal performance is discussed. In this regard, a semiempirical correlation is described that relates influence coefficients derived from the isolated inlet tests to measured (or calculated) forebody flowfields to predict installed inlet internal performance characteristics. Predicted performance is then compared with measured installed inlet performance to establish the suitability of the correlation.

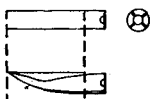
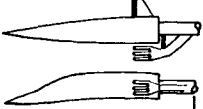
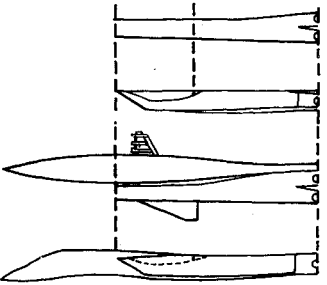
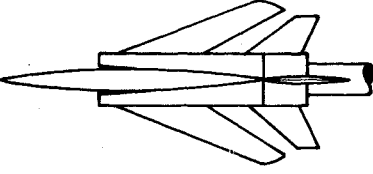
The data presented were derived from a specific configuration, but the principles employed in the correlation are generally applicable. They suggest a basis for building from the available body of wind-tunnel data a semiempirical theory to predict installed performance for a number of different configurations. Where such wind-tunnel data do not exist, the integrated aeropropulsion wind-tunnel approach used in this investigation might serve as an example of how to obtain the required data systematically.

Wind-Tunnel Program

The approach used in development of the inlet/airplane integration is depicted in Table 1. The inlet is a side-mounted, horizontal ramp, four-shock, external compression design. All models feature changeable forebody, diverter, and inlet parts. To relate and directly use the wind-tunnel results in the over-all system performance validation, a reference airplane was established in the aeropropulsion drag model. Thus, all changes made to the configuration to improve inlet internal performance had to be incorporated into the reference model and tested. Conversely, all changes made in the reference configuration had to be incorporated in the inlet models. Close coordination, then, was achieved in an alternating sequence of testing, wherein aerodynamic test results were used in planning inlet tests, and inlet test results were used to determine the next phase of forebody development for aerodynamic tests.

The inlet performance objectives achieved in the wind-tunnel program included: 1) Develop a high-performance, external

Table 1 Summary of wind-tunnel tests

Test	Sketch of Model	Test Date	Test Facility	Objectives
Inlet Alone (Short Diffuser)		Nov. 17 - Dec. 17, 1969	Boeing 18" x 18" Free-Jet Tunnel	1. Inlet Performance Evaluation at α 2. Boundary Layer Bleed System Development 3. Evaluate Side-Plate Shapes 4. Evaluate Cowl Lip Shapes 5. Measure Buzz Limit
Supersonic Flowfield Survey		Jan. 9 - 21, 1970	Boeing 4' x 4' Supersonic Wind Tunnel	1. Obtain Extensive Flowfield Measurements at the Inlet Station
Inlet Alone (Long Diffuser)		Feb. 9 - 13, 1970	Boeing 8' x 12' Transonic Wind Tunnel	1. Evaluate Inlet Performance and Distortion at α and β 2. Correlate Flowfield Measurements with Measured Inlet Performance
and		Feb. 24-27, 1970	Boeing 4' x 4' Supersonic Wind Tunnel	3. Evaluate Installed Inlet Performance in the Airplane Flowfield at α and β for Supersonic and Transonic Mach Numbers
Inlet Plus Forebody (and Partial Wing)		Apr. 15 - 30, 1970	Boeing 4' x 4' Supersonic Wind Tunnel	4. Investigate Boundary Layer Diverter Height
Aero-Propulsion Drag Model		Dec. 12-23, 1969	Boeing 8' x 12' Transonic Wind Tunnel	1. Measure Drag for Total Airplane
		Apr. 27-May 13, 1970	Boeing 8' x 12' Transonic Wind Tunnel	2. Investigate Effects of Variations in Configuration Geometry
		May 26-June 5, 1970	Boeing 4' x 4' Supersonic Wind Tunnel	

compression, two-dimensional inlet (inlet alone). 2) Measure the flowfields produced at inlet station by a variety of fuselage forebody shapes. Upwash, outwash, and local Mach number distributions were measured. 3) Measure performance of installed inlet. The inlet was installed on the forebody, and its performance determined in the flowfields produced by the forebody for a number of shape variations, inlet orientations (toe-in and cant), and vertical displacement. 4) Correlate experimentally measured installed-inlet performance with measured flowfields and inlet alone measurements.

Results

Three basic test models were used to gather inlet alone, forebody flowfield, and installed data. The test models and results from each test series are discussed in the following sections.

Inlet Alone Test

This model, illustrated in Fig. 1, was designed to develop the supersonic diffuser. The model was provided with a wide range of variability in cowl shape, sideplate shape, ramp, sidewall, and cowl porosity for boundary-layer bleed system development. It featured three remotely actuated, movable ramps for variations in shock geometry and throat area. Several variations in ramp bleed systems were provided, including both porous panels and slots. A fairly short subsonic diffuser was provided upstream of the single compressor face. The model was tested in the Boeing Propulsion Laboratories' 18- by 18-in. Free-Jet Tunnel at Mach numbers from 1.40 to 2.40.

There was extensive effort in developing the shock geometry and boundary-layer bleed system. After evaluating several different configurations, the throat slot was selected as the best bleed configuration. Fifty percent cutback sideplates were

also selected. This configuration provided a combination of good inlet recovery characteristics, adequate buzz margin, high pressure recovery in the bleed plenum, and simplicity (no bleed was required other than a wide throat slot). The selected configuration was further developed to the point where a high performance level was achieved (matched at the Mach 2.20 flight condition for a representative turbofan engine airflow). Figures 2-4 represent typical performance obtained. These results were used, as shown in the figures to obtain the effects of yaw angle, angle of attack, and local Mach number on inlet recovery for constant ramp angle settings. The effects vary considerably as inlet mass flow ratio is changed. Thus, the data were presented as a function of airflow for a variety of constant corrected airflows, $W(\theta_2)^{1/2}/\delta_2$. This allowed derivation of sensitivity changes with basic inlet performance level and airflow. The region of most likely matching airflow has been cross-hatched to indicate where a high-performance inlet could be expected to operate.

The effect of Mach number gradient in the inlet local flowfield (Fig 5) was generated from data obtained from other tests and published reports. The cross hatched area represents the approximate bandwidth of the available data.

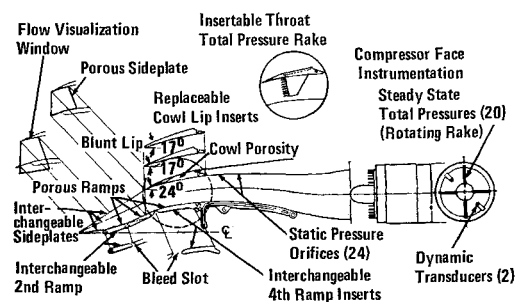


Fig. 1 Wind-tunnel model used to develop supersonic inlet.

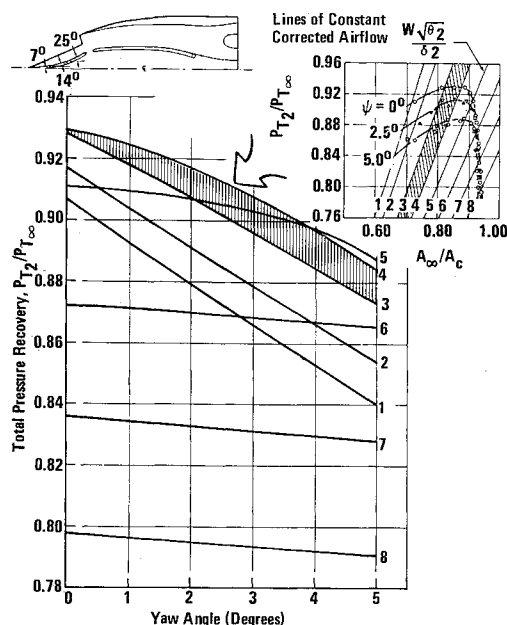


Fig. 2 Effect of yaw on inlet recovery at constant ramp angles.

Forebody Flowfield Test

Detailed flowfield measurement were taken at the inlet station using a group of nine 40° cone probes calibrated and fixed at the tunnel centerline. The forebody model and boundary-layer rakes were designed so they could be positioned in relation to the cone probes without disturbing their location in the tunnel. In this way, the Mach number was determined within ± 0.02 and flow angularity within $\pm 0.15^\circ$.

The forebody shapes tested are shown in Fig. 6, as derived from the model templates. The basic forebody (Model 1) was derived from the configuration drawing. Models 2 and 3 were derived from Model 1 by wax fairings to match the body shapes shown.

Results were obtained at a tunnel Mach number of 2.2, angles-of-attack from -4° to 16° , and angles-of-sideslip from -4° to $+4^\circ$ at 0° , 5° , and 10° angles-of-attack. The

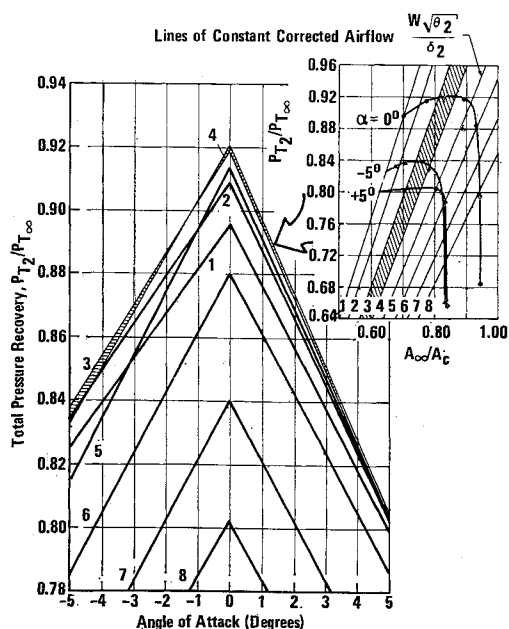


Fig. 3 Effect of angle-of-attack on inlet recovery at constant ramp angles.

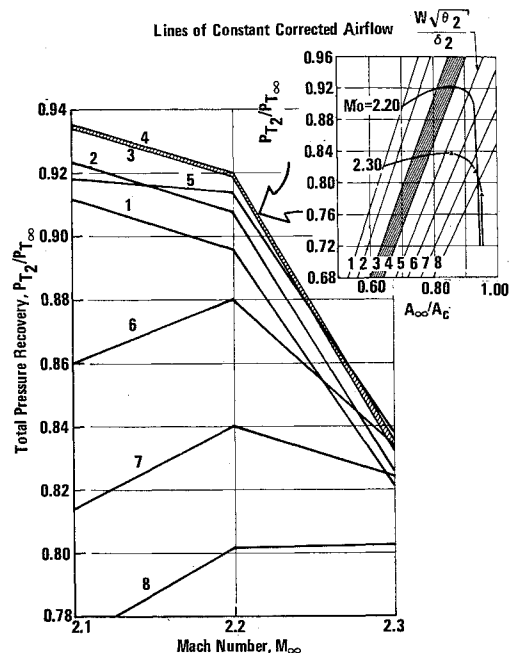


Fig. 4 Effect of local Mach number on inlet recovery at constant ramp angles.

unit Reynolds number was approximately $8.4 \times 10^6/\text{ft}$. A typical set of data derived from these results and used in the correlation analysis is shown in Fig. 7.

Installed Inlet/Forebody Tests

Following completion of the inlet alone and the forebody flowfield tests, the inlet was tested with the forebody installed as shown in Fig. 8. The forebody was removable for obtaining inlet alone performance data.

The forebody shape variations were the same as used in the flowfield tests. However, some additional variations were included besides those shown in Fig. 6. The forebody nose inclination and over all inclination relative to the inlet could

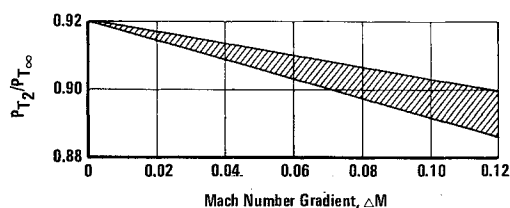


Fig. 5 Effect of local Mach number gradient on inlet recovery.

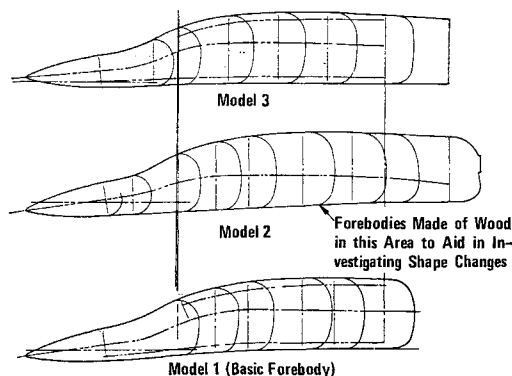


Fig. 6 Basic forebody shapes used in study.

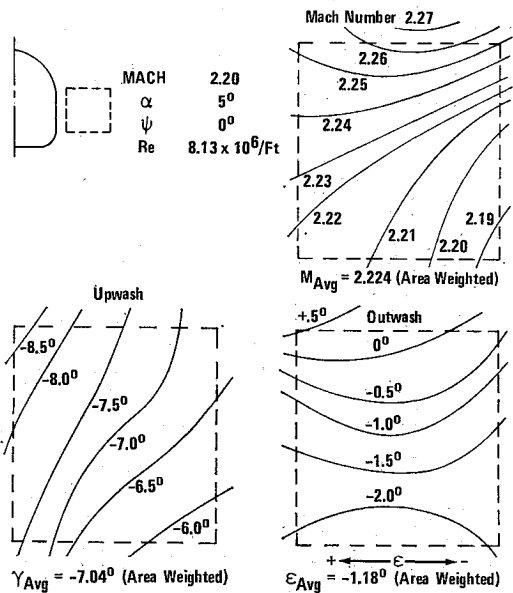


Fig. 7 Typical measured forebody flowfield data.

be varied as show in Fig. 9. The inlet position variation built into this model allowed for vertical displacement, toe-in, and diverter width adjustment.

During tests with the forebody installed, significant changes in the inlet alone performance were observed. Some of the more significant results are presented in Figs. 10–15. Smoothing out the canopy forward bump (Fig. 10) was found to have negligible effect on the inlet performance. The design angle-of-attack for the airplane was +5°, and this, together with the remote location of the inlet relative to the canopy, apparently caused the effect of the canopy compression to pass over

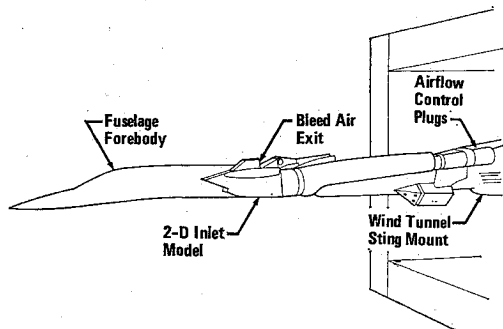


Fig. 8 Inlet/forebody model installed in 4' x 4' supersonic wind tunnel.

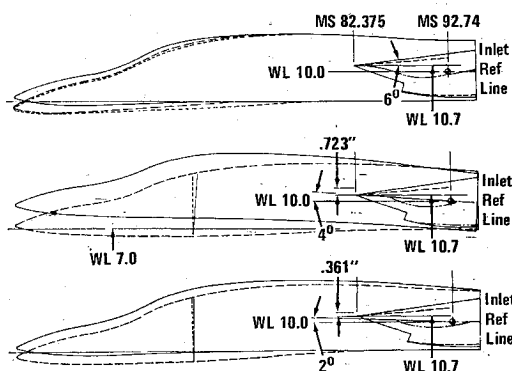


Fig. 9 Variations in forebody orientation used in tests.

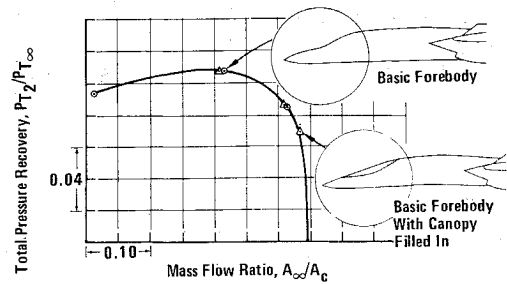


Fig. 10 Effect of smoothing out canopy on inlet performance.

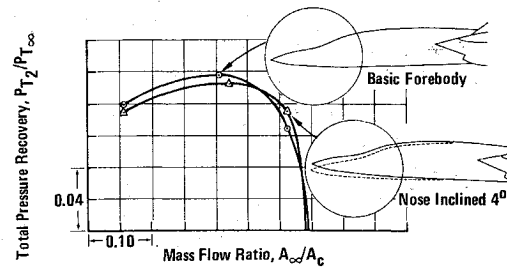


Fig. 11 Effect of nose inclination on inlet performance.

the inlet. Likewise, tilting up the forward part of the forebody nose 4° had only a small effect (Fig. 11).

Moving the inlet down from the basic location, however, was found to result in a significant improvement in recovery. This is due primarily to the lower local Mach number in this location. Fig. 12 compares inlet performance in the two locations.

The most dramatic improvement in inlet performance was achieved by rotating the forebody up 4° ahead of the inlet. This eliminated the expansion due to the drooped nose, and placed the inlet in a flowfield where the local Mach number was close to its design value. The effects of both positive and negative inclination of the forebody are shown in Fig. 13.

During the early part of the test program, several test runs indicated that the general level of installed inlet recovery for the basic forebody shape, orientation, and location was

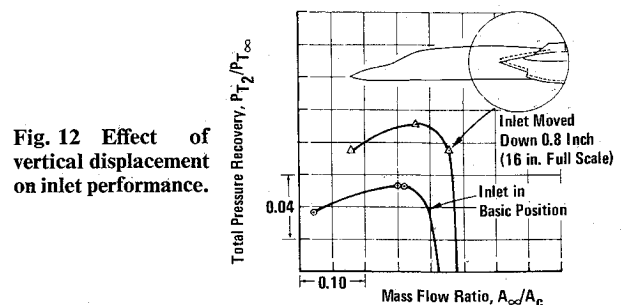


Fig. 12 Effect of vertical displacement on inlet performance.

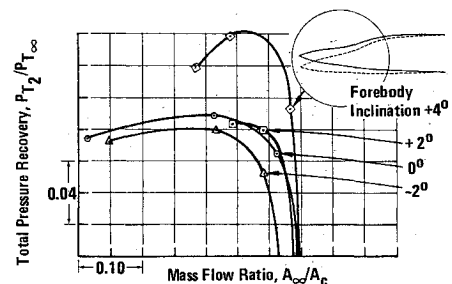


Fig. 13 Effect of forebody inclination on inlet performance.

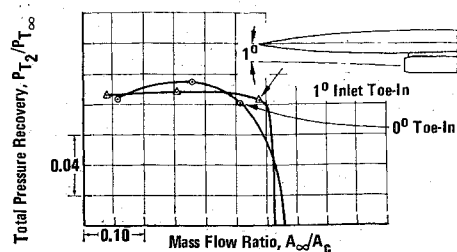


Fig. 14 Effect of toe-in on inlet performance.

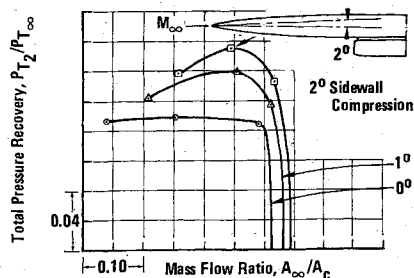


Fig. 15 Effect of sidewall compression on inlet performance.

approximately 4% lower than the inlet alone recovery. This provided a great stimulus to investigate ways to improve the installed recovery. These variations include toe-in and sidewall compression. The results from forebody flowfield tests indicated that approximately 1° of outwash could be expected at the inlet station. A test was made to determine the improvement in inlet recovery obtainable by aligning the inlet more perfectly with the local flow direction. The result of 1° inlet toe-in is shown in Fig. 14. It resulted in approximately 1% improvement in recovery at the mass flow ratio where the inlet would match the engine. Increasing the sidewall compression also had a significant beneficial effect on inlet performance. Figure 15 shows that an improvement of 4.2% in inlet recovery can be achieved by increasing the sidewall compression by 2°.

Correlation of Results

The first phase of installed inlet testing revealed major deviations from the predicted isolated inlet performance. This was particularly noteworthy by contrast with the excellent agreement obtained between theory and experiment in the inlet alone series. Consequently, an attempt was made to relate the isolated inlet performance results to the measured local properties of the installed inlet flowfield. This would provide a guide in understanding the relative magnitude of the factors in the installation creating losses in inlet performance. It would also establish a basis for generalizing the results obtained for this configuration so they can be applied to other configurations.

Empirical influence coefficients were derived from the isolated inlet results and combined with measured flowfield factors to predict installed performance. The influence coefficients selected are shown in Fig. 16. Note that the product of the coefficient and corresponding flow property produces the incremental change in inlet recovery due to that nonuniform flow influence in the installed environment. In other words, a linear superposition of uniform flowfield changes such as angle of attack, yaw, and local Mach number derived from the inlet alone results (Figs. 2-4), along with the Mach gradient correlation (Fig. 5) are assumed to account for the total nonuniform flow effect. Average properties of the actual flowfield, as typified in Fig. 7, are used in this relationship.

$$\begin{aligned} \left(\frac{P_{T2}}{P_{T\infty}} \right)_{\text{Installed}} &= \left(\frac{P_{T2}}{P_{T\infty}} \right)_{\text{Inlet Alone}} + \left[\frac{\partial (P_{T2}/P_{T\infty})}{\partial \alpha} \right]_{\text{Inlet Alone}} \times (\sigma_T)_{\text{Forebody}} \\ &+ \left[\frac{\partial (P_{T2}/P_{T\infty})}{\partial M_L} \right]_{\text{Inlet Alone}} \times (\Delta M_L)_{\text{Forebody}} + \left[\frac{\partial (P_{T2}/P_{T\infty})}{\partial \psi} \right]_{\text{Inlet Alone}} \times (\epsilon_T)_{\text{Forebody}} \\ &+ \left[\frac{\partial (P_{T2}/P_{T\infty})}{\partial \Delta M} \right]_{\text{Inlet Alone}} \times (\Delta M)_{\text{Forebody}} + \left(\frac{\Delta P_{T2}}{P_{T\infty}} \right)_{\text{Interactions, Boundary Layer Ingestion Effects, and Other Unexplained Effects}} \end{aligned}$$

Fig. 16 Correlation of installed inlet performance using measured flowfield data.

However, as shown in Figs. 2-4, there is a significant variation in the influence coefficient depending on the maximum performance level of the inlet and the airflow demand. (Note: In this study, the inlet was designed to have maximum performance at $M_\infty = 2.2$ and $\alpha = 0$ thus, the linearly extrapolated data show abrupt changes at these values of M_∞ and α). In general, the lower performance region of the inlet operation tended to have less sensitivity to flowfield effects than at the higher performance. Thus, it is important to have a high-performance inlet when tests of installation effects are being made, otherwise results may be misleading. For these reasons, the influence coefficients were obtained within the cross hatched region of data presented in Figs. 2-5. This region represented the high-performance engine-inlet airflow matched condition with negligible boundary-layer ingestion. The resulting influence coefficients are summarized in Table 2.

Two examples are presented from the several cases analyzed to illustrate the application of the method described in Fig. 16. The first example is for the inlet and fuselage in the basic (Model No. 1, Fig. 7) condition. The results are shown in Fig. 17. Very good agreement with the measured installed results was obtained in this case. In general, the method

Table 2 Experimentally derived influence coefficients

Influence Coefficient		Configuration No. 1 Sharp Cowl Lip 50% Sideplates Ramp Angles: 7,14,25° Mo = 2.20 Design Point			
Effect of Upwash	$\partial \left\{ \frac{P_{T2}}{P_{T\infty}} \right\}$ $\partial \alpha$	$\alpha = -5 - 0^0$	$\alpha = 0 - +5^0$		
		+ 0.0175	- 0.0252		
Effect of Local Mach Number	$\partial \left\{ \frac{P_{T2}}{P_{T\infty}} \right\}$ ∂M_L	ML = 2.10 - 2.20	ML = 2.20 - 2.30		
		- 0.0015	- 0.0082		
Effect of Sidewash	$\partial \left\{ \frac{P_{T2}}{P_{T\infty}} \right\}$ $\partial \psi$	$\psi = 0 - 1^0$	$\psi = 1 - 2^0$	$\psi = 2 - 3^0$	$\psi = 3 - 4^0$
		- 0.007	- 0.009	- 0.0105	- 0.0115
Effect of Mach Number Gradient	$\partial \left\{ \frac{P_{T2}}{P_{T\infty}} \right\}$ $\partial \Delta M$	$\Delta M = 0 - .10$			
		- 0.228			
Interactions, Boundary Layer Ingestion Effects, and Other Unexplained Effects		$\left\{ \frac{\Delta P_{T2}}{P_{T\infty}} \right\}$ Varies From 0 - 0.0135			

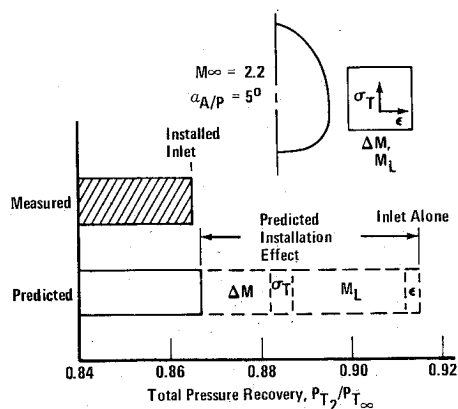


Fig. 17 Comparison of predicted and measured installed inlet performance data for basic forebody shape and orientation.

produced agreement within 1% of inlet recovery for other similar cases.

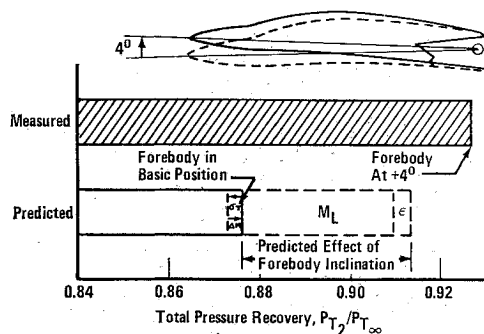


Fig. 18 Comparison of predicted and measured effect of forebody inclination.

The second example was for the Model 2 forebody inclined 4° from basic position. As shown in Fig. 18, the agreement was still within 1% recovery, thus showing the general validity of the method relative to this set of data. Other airplane configurations should be analyzed in similar fashion and compared with installed measurements before general application of the method is warranted. However, present results are very encouraging relative to developing an empirical prediction scheme.

Conclusions

- 1) Inlet performance was found to be very sensitive to small changes in forebody shape within a limited region ahead of and below the inlet. Changes in recovery of as much as 5–7% were produced by relatively minor variations in local contours and angles within this region.
- 2) Inclination of the forebody ahead of the inlet was found to substantially affect local flowfield conditions, resulting in greatly changed pressure recovery. Five to six percent change in recovery was achieved as a result of $+4^{\circ}$ inclination.
- 3) Changes in the shape and inclination of the forward (nose) part of the forebody ahead of the canopy produced little effect on inlet performance. Smoothing out the forward canopy step also had negligible effect on inlet performance. These effects were influenced by the fact that for this configuration, the inlet was located relatively far aft of the forebody nose and canopy.
- 4) A strong correlation was found between incremental changes in local Mach number due to forebody shape and inlet performance. This trend correlates well with inlet alone performance.
- 5) Empirical influence coefficients were found to offer a useful approach for correlating installed inlet recovery data. They should be further investigated by applying the approach to the extensive body of flowfield and installed inlet test data currently available from recent test programs.
- 6) Additional study should be made to establish, from recent test results on inlet performance a better representation of the effects of Mach number gradients in the flowfield ahead of the inlet.